I-V modeling of current limiting mechanisms in HgCdTe FPA detectors

A. Scotty Gilmore*[a], James Bangs[a], Amanda Gerrish[a]

[a]Raytheon Vision Systems, 75 Coromar Dr. Building 1, Goleta, CA 93117.

ABSTRACT

This paper details significant improvements in current-voltage (I-V) modeling capabilities using an automated iterative non-linear fitting program. The properties of a particular infrared (IR) detector's I-V curve are dependent upon the current limiting mechanisms in the device which depend upon the temperature, applied bias, and cutoff wavelength or detector bandgap. This model includes ideal diode diffusion, generation-recombination, band-to-band tunneling, trap-assisted tunneling, shunt resistance, and avalanche breakdown as potential current limiting mechanisms in an IR detector diode. The modeling presented herein allows one to easily distinguish, and more importantly to quantitatively compare, the amount of influence each current limiting mechanism has on various detector's I-V characteristics. Modeling of the trap-assisted-tunneling mechanism leads to an estimate of the density of occupied trap states at a given temperature. This model is now routinely applied to Raytheon Vision Systems' test structures to better understand detector current limitations.

Keywords: HgCdTe, IV, Modeling, Trap-assisted Tunneling

1. INTRODUCTION

Current state of the art HgCdTe infrared imaging often requires near background limited performance (BLIP) at low operating temperatures. Due to the low background photon flux in space based strategic applications, the limiting parameter for these devices becomes the leakage current. With low background irradiances, BLIP noise equivalent irradiances (NEQ) must be on the same order, reducing leakage currents to the picoamp level as shown in figure 1. As allowable leakage currents decrease, an understanding of the mechanisms contributing to the leakage current becomes necessary. Deconstructing the total observed leakage current into its component parts allows identification, and possible minimization, of the dominant current limiting mechanism.

Long wavelength IR detectors operating at low temperatures are characterized by a narrow band gap allowing tunneling to act as the dominant current limiting mechanism. One signature of this effect is revealed in a semilog plot of R_0A against inverse temperature as shown for a typical detector in figure 2. Asymptotic lines in the plot represent modeled diffusion limited and generation-recombination (G-R) limited current behavior. At room temperature, this device follows the diffusion limited trend, then as the temperature is lowered, it becomes G-R limited, and finally it deviates completely from both the diffusion and G-R behaviors. This final deviation at lower temperatures is attributed to tunneling, but it is not well understood. Quantification of the tunneling parameters relevant to IR detector performance through modeling is the main thrust of this paper. This I-V modeling is applicable to a broad range of cutoff wavelengths and operating temperatures. All samples modeled herein share a common n-p^+ diode structure shown in figure 3.

*angelo_s_gilmore@raytheon.com; phone 1 805 562-4398; fax 1 805 562-2948; Raytheon.com

Infrared Systems and Photoelectronic Technology, edited by Eustace L. Dereniak, Robert E. Sampson, C. Bruce Johnson, Proceedings of SPIE Vol. 5563 (SPIE, Bellingham, WA, 2004) · 0277-786X/04/$15 · doi: 10.1117/12.562614

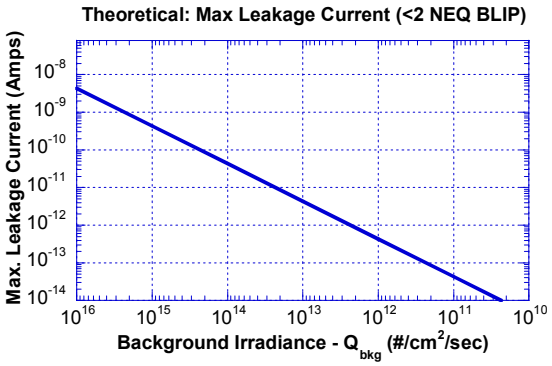

Fig. 1. Leakage current versus background irradiance at 40K.

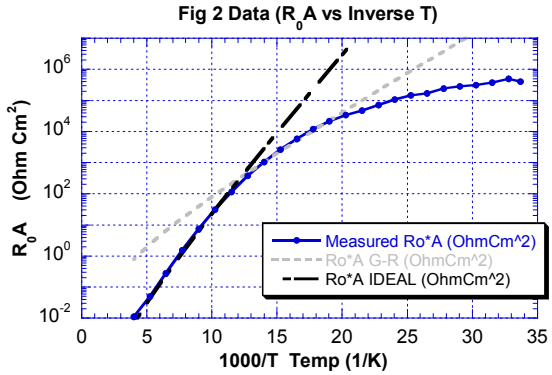

Fig. 2. R_0A versus inverse temperature for a long-wave infrared (LWIR) detector diode.

2. MODEL

The I-V curve fit programs developed at RVS implement an iterative fit of the basic equations for current in a semiconductor diode to $Hg_{1-x}Cd_xTe$ current-voltage data. These equations include terms for diffusion limited current (an ideal diode), generation-recombination current, band-to-band tunneling, trap-assisted tunneling, a surface leakage shunt resistance and avalanche breakdown. These programs can be operated in stand-alone configurations which incorporate a user-friendly interface to allow analysis of I-V data stored in Excel files. The programs can also be run in batch mode configuration which uses a different interface to extract and fit I-V data from an internal database, and then stores the fitted parameters back into this database for later analysis. For the stand-alone configuration, data may be read in from an Excel file which has the I-V data in one of two formats – fixed temperature or multiple temperatures. The fitting procedure uses a standard non-linear gradient-search method for minimizing the chi-squared error (fit variance) between the data and the fitted function[1]. A parabolic expansion of the chi-squared surface is used to speed up convergence as the parameters approach the optimal solution. Fitting all 14 free parameters in the current equations was problematic because of the tendency of the algorithm to converge on local minima. In order to obtain a more robust fit, we found it necessary to fit the various current terms in a sequential fashion. The various current components are fit in the bias region in which they have the most influence on the fit. If a parameter variation yields no minimization of the fit variance, then that parameter is excluded from the fit for the particular diode being modeled in an attempt to minimize the number of free variables and increase the physical applicability of the model. The specifics of the current limiting parameters used in the modeling are detailed below.

3. CURRENT LIMITING PARAMETERS

The models used contain within them one or more variables related to each incorporated current limiting mechanism. In an ideal IR detector, a diffusion limited current would exist under operating conditions. In this "ideal diode" case, both a small leakage current, I_{lk}, and high resistance, R_0A, figures of merit would be obtained. However, in practice, crystalline defects and impurities create trapping sites in the device leading to recombination or trap-assisted tunneling. Even in a perfect crystal of LWIR or VLWIR HgCdTe material, the semiconductor electronic bandgap is often less than 100meV at operating temperatures. This, combined with standard operating conditions of a slight reverse bias, leads to a higher probability of band-to-band tunneling events. Individually or combined, these recombination and tunneling mechanisms have the potential to significantly limit the detector performance, increasing the leakage current and reducing the R_0A factors. Figure 3 shows a cartoon of a typical diode structure (left side of figure) and the major current limiting mechanisms operating on this diode (right side of figure). In this section, each of the main current limiting mechanisms is briefly described along with its relevance to HgCdTe IR detector devices.

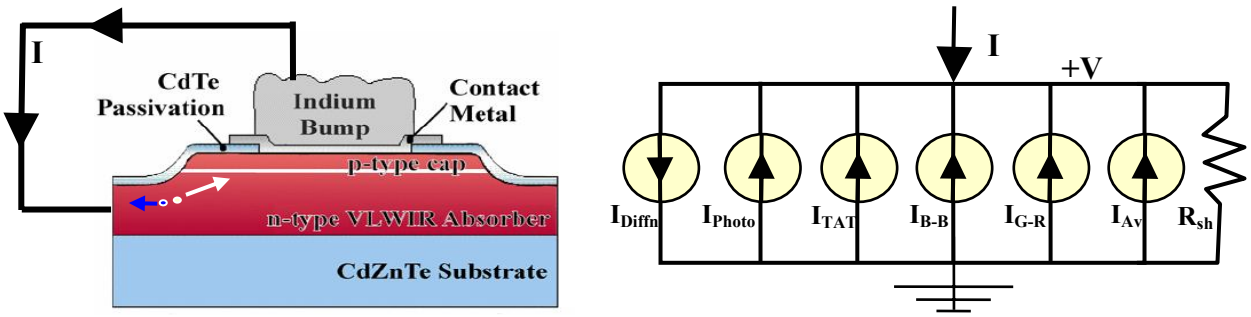

Fig. 3. Left side is a cartoon of the diode structure at RVS. Right side shows possible currents operating in the device. I_{Diffn} is the ideal diffusion current, I_{Photo} is the photogenerated current, I_{TAT} is the current due to trap-assisted tunneling, I_{B-B} is due to band-to-band tunneling, I_{G-R} is due to generation or recombination mechanisms, I_{Av} is due to avalanche breakdown, and R_{sh} is due to surface leakage shunt resistance. Limiting currents act in opposition to the diode diffusion current.

3.1 Diffusion

This is the ideal current transfer mechanism for a diode. This assumes that currents are limited only by thermal diffusion rates through the material. The ideal diode equation is given by

$$I_{Diff} = I_0 * \left(1 - Exp\left[\frac{V - IR_S}{nk_BT}\right]\right), \quad \text{where} \tag{1}$$

$$I_0 = Aq\left(\frac{D_e n_{ip}^2}{L_e N_A} + \frac{D_h n_{in}^2}{L_h N_D}\right). \tag{2}$$

I_0 is the reverse bias saturation current, R_S accounts for any parasitic series resistance in the device, n is the ideality factor, V is the applied voltage, k_B is Boltzman's constant ($k_B = 8.6\text{x}10^{-5}$eV/K), T is the temperature, A is the area of the diode, q the charge of an electron ($q = 1.6\text{x}10^{-19}$C), n_{ip} and n_{in} are the intrinsic carrier concentration in the p-type and n-type layers, D_e the electron and D_h the hole diffusion coefficient, L_e the electron and L_h the hole diffusion length, and N_A the acceptor and N_D the donor density. In a homojunction, $n_{ip} = n_{in} = n_i$, and in an n-p^+ diode, $N_A >> N_D$. The series resistance should be minimized and the ideality factor should be near unity for ideal diffusion behavior.

Diffusion dominates the current properties under forward bias (positive applied bias applied to the p-type layer), allowing the variables (R_S, n, I_0) to be fit to the current-voltage characteristics in the forward bias regime. Typical detector diodes are diffusion limited at higher temperatures, as seen in figure 2.

3.2 Generation-recombination (G-R)

Carriers in the depletion region may either be generated through spontaneous electron-hole pairing or recombined, through Schottky Read type recombination centers. Recombination processes limit the standard diffusion current in HgCdTe IR devices under the condition of reverse bias where $pn << n_i^2$. Here, p and n are the non-equilibrium hole and electron concentrations under reverse bias. Under these non-equilibrium conditions, emission processes will dominate in an attempt to return the system to equilibrium. Current generated by such emission is given by[2]

$$I_{Gen} = \frac{qAn_i w_d}{\tau_e}. \tag{3}$$

Equation 3 contains τ_e, the effective carrier lifetime in the depletion layer and w_d, the depletion width. The depletion width of a step junction introduces the main voltage dependence in this generated current as

$$w_d = \sqrt{\frac{2\varepsilon_s (V_{bi} - V)}{q}\left(\frac{1}{N_A} + \frac{1}{N_D}\right)}, \tag{4}$$

$$\text{where } V_{bi} = \frac{k_BT}{q} Ln\left[\frac{N_A N_D}{n_i^2}\right]. \tag{5}$$

In equations 4 and 5, ε_s is the semiconductor dielectric constant and V_{bi} is the built in voltage. For an n-p^+ junction, equations 3, 4, and 5 can be combined to yield

$$I_{Gen} \cong \frac{qAn_i}{\tau_e}\sqrt{\frac{2\varepsilon_s}{qN_D}}\sqrt{(V_{bi}-V)} = Amp_{Gen}\sqrt{(V_{bi}-V)}. \quad (6)$$

Amp_{Gen} in equation 6 includes all the voltage independent prefactor terms. Since equation 3 is only valid for reverse bias conditions, the parameter Amp_{Gen} is obtained through fitting equation 6 to the data in the reverse bias region. Generation-recombination processes have more influence in $Hg_{1-x}Cd_xTe$ IR detector performance at lower temperatures and higher x values. This temperature dependence can be seen in the example shown in figure 2.

3.3 Band-to-Band Tunneling:

Electrons (holes) in the depletion region may tunnel directly from occupied states in the valence (conduction) band to unoccupied states in the conduction (valence) band or vice versa provided there is no net change in the energy of the carrier. This is made possible due to a slight band overlap under reverse bias conditions. This is detailed in figure 4A. An equation describing the current flow due to band-to-band tunneling [2] is:

$$I_{btb} = \frac{\sqrt{2m_e}q^3AEV}{4\pi^2\hbar^2E_g^{1/2}}\exp\left[-\frac{4\sqrt{2m_e}E_g^{1/2}}{3qE\hbar}\right], \quad (7)$$

$$E = \sqrt{\frac{qN_D(V_{bi}-V)}{2\varepsilon_S\varepsilon_0}}\text{, and } E_{\max} = \sqrt{2\frac{qN_D(V_{bi}-V)}{\varepsilon_S\varepsilon_0}} \quad (8)$$

where E is the electric field strength in the p-n junction, E_g is the bandgap, hbar is Plank's constant over 2π, m_e is the effective mass of an electron. The maximum electric field in an n-p^+ junction is assumed in this paper, and is given above in equation 8. Combining and simplifying equations 7 and 8 yield

$$I_{btb} = Amp_{btb}V(V_{bi}-V)^{m_{btb}}Exp\left[\frac{Rate_{btb}}{(V_{bi}-V)^{m_{btb}}}\right] - \frac{V}{R_{shunt}}, \quad (9)$$

where V_{bi} is the built in voltage due to the band bending in the depletion region of the p-n junction, R_{shunt} is a shunting resistance, Amp_{btb} is a voltage independent constant related to the quantity of tunneling events, and $Rate_{btb}$ is a constant related to the tunneling rate between the valence and conduction bands. Equation 9 has incorporated both a slight variation of the power dependence of the electric field, m_{btb}, from the typical value of 1 (giving a voltage dependence of ½) as done by Chynoweth[3] as well as the inclusion of the shunt resistance term. The variable parameters used in the model are therefore Amp_{btb}, $Rate_{btb}$, m_{btb} and R_{shunt}. Equation 5 allows the calculation of the built in voltage, estimating the intrinsic carrier concentration for $Hg_{1-x}Cd_xTe$ as[4]

$$n_i(E_g,T) = \left(5.585 - 3.820x + 1.753(10^{-3})T - 1.364(10^{-3})Tx\right)*\left[(10^{-3})E_g^{3/4}T^{3/2}Exp\left(\frac{-E_g}{2k_BT}\right)\right] \quad (10)$$

where x is the cadmium concentration and E_g is the semiconductor bandgap. Both the band-to-band tunneling and shunt resistance terms are fit to the middle reverse bias region.

3.4 Trap-assisted-tunneling (TAT)

Trapping states provide centers for tunneling between bands allowing trap-assisted tunneling to occur. Figure 4 contains a schematic of this process. An energetic transition occurs from an initially occupied energy band site to a trapping site, followed by a zero energy tunneling event from this trapping site to the final energy band. Traps "assisting" in the tunneling process in this manner, allow a larger portion of the material to participate in tunneling events than band-to-band tunneling alone could account for. Transition probability rates have been derived by Chynoweth[3,5] and Price[6], and later advanced by Sah[7], with a more robust derivation of TAT applied to $Hg_{1-x}Cd_xTe$ detectors by Kinch[8]. These transition rates determine the current induced by trap-assisted tunneling, and have been used by several authors[9,10,11,12,13] to model TAT in $Hg_{1-x}Cd_xTe$. The current can be modeled in one dimension as:

$$I_{TAT} = qAN_t w_d TAT_{probabiliy}, \quad (11)$$

$$TAT_{probability} = \frac{\pi^2 qm_eEM^2}{\hbar^3(E_t')}\exp\left[-\frac{4(2m_e)^{1/2}(E_t')^{3/2}}{3\hbar qE}\right], \quad (12)$$

where N_t is the trap density, and $TAT_{probability}$ is the tunneling rate of electrons. Equation 12 contains m_e, the effective mass of an electron assumed to be[8] $m_{ex}= m_{ey} = m_e = 0.07*E_g*m_0$, hbar which is Plank's constant over 2 Pi, ε_S, the dielectric constant here assumed to be $(19.7\text{-}10.5x)\varepsilon_0$ where x is the Cd concentration from $Hg_{1-x}Cd_xTe$, and q, V_{bi}, E_g, and N_D which are the same as above. E_t' is the energy difference between the trapping state level and the relevant energy band. For capture of a conduction electron in an acceptor level, $E_t' = E_t\text{-}E_C$; and for emission of an electron to the valence band from a donor level, $E_t' = E_t\text{-}E_V$. In equation 12, E is the electric field at the trap site in the depletion width, and M is defined by Sah[7] as a "matrix element for electron tunneling out of the trap to the valence band" an average of which was determined experimentally for gold doped silicon to be $M^2(m_e/m_0)=10^{-23}cm^3V^2$ for Si, which is used here and elsewhere[9,10,11,12,13] as a rough estimate of the same quantity for $Hg_{1-x}Cd_xTe$.

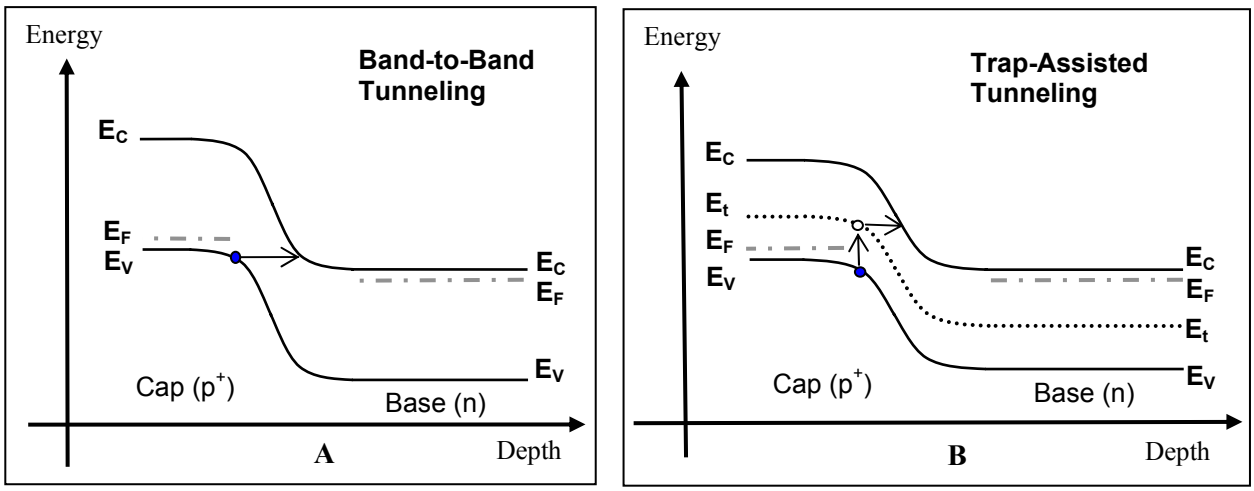

Fig. 4. Energy band diagrams for $Hg_{1-x}Cd_xTe$ illustrating tunneling processes. The offset between the Fermi levels in the n-type and p-type layers is due to a small reverse bias simulating detector operating conditions. Clear circles represent trapping states, filled circles represent electrons. A) Band diagram is for possible band-to-band tunneling transition. B) Band diagram is for possible trap-assisted-tunneling transition.

Assuming the maximum electric field strength, and combining equations 8, 11, and 12, immediately yields

$$I_{TAT} = Amp_{TAT}(V_{bi} - V)\exp\left[-\frac{Rate_{TAT}}{(V_{bi} - V)^{1/2}}\right]. \quad (13)$$

where Amp_{TAT} and $Rate_{TAT}$ are voltage independent terms assumed constant over the applied bias range of a typical I-V measurement set. From equation 13, it is clear that two variable parameters exist in the modeling of the TAT effect. From these two parameters, tentative estimates of E_t' and N_t can be made. These are tentative due to the unknown estimates of the M value, the fact that the maximum electric field strength was assumed for all tunneling events, and the depletion width was assumed to be the entire depletion width, which is an overestimate as the majority of the tunneling events will occur in the vicinity of the maximum electric field strength. However, keeping those limitations in mind, variations in these modeled quantities (and hence the extracted E_t' and N_t) from sample to sample will still yield valuable information.

Trap-assisted tunneling has the largest contribution to the measured current near the zero applied reverse bias region, hence Amp_{TAT} and $Rate_{TAT}$ are fit to the data in this range. Both band-to-band tunneling and trap-assisted tunneling mechanisms have higher contributions to the measured current in a HgCdTe IR detector diode at lower temperature. Figure 2 clearly shows deviation from either diffusion limited or generation recombination limited behavior at lower temperatures as tunneling mechanisms begin to dominate the current.

3.5 Avalanche breakdown

Avalanche breakdown is mainly seen at high reverse bias (>-500mV), so it does not typically affect detector performance under operating conditions. However, it was included in this model both as a physical check and to ensure comprehensive applicability. The current due to avalanche breakdown[2] can be modeled as

$$I_{AvBr} = \frac{I_{LK}}{1-(V/V_{Br})^N}, \tag{14}$$

where I_{LK} is the leakage current due to all the other current limiting mechanisms stated above, V is again the applied bias, and V_{Br} is the breakdown voltage. Application of a bias much less than the breakdown bias returns a value of I_{LK}, as expected. A similar equation using the depletion width rather than V, and an electron impact ionization coefficient ($\alpha_e=\alpha_0 \exp[-b/E]^m$) rather than $1/V_{Br}$ has also been reported[14], but for the purposes of this research, this simple model was found to be sufficient. The typical value for N is ½, but this can be slightly different depending on failure mechanism, so it is considered a variable parameter in this modeling.
The main variable in this mechanism is V_{Br}, the breakdown voltage, which is typically several hundred millivolts, and is fit to the large reverse bias region I-V data. Operation of HgCdTe IR detectors is performed under a slight reverse bias, where this breakdown effect has little to no influence.

4. RESULTS

Application of this modeling program to HgCdTe detector mini-array test diodes is now standard procedure at Raytheon Vision Systems. Here, a few typical examples will be presented to show some of the applications for this model. Modeled avalanche breakdown terms were found to be insignificant for the applied bias range of interest, and will be neglected in this discussion. Data corresponding to a typical I-V curve for a long wavelength IR detector diode (same as figure 2) at a temperature of 40K is represented by the solid triangles in figure 5. Model generated fits to the data are also included in the figure, represented by the solid lines. The step-by-step graphical representation of the main current limiting mechanisms are displayed including diffusion (5A), trap-assisted tunneling (5B), and band-to-band tunneling (5C). When combined, along with the remaining modeled parameters shown in table 1, they yield an excellent fit, shown in figure 6. Also included in figure 6 is the measured data and model fit at 78K for comparison.

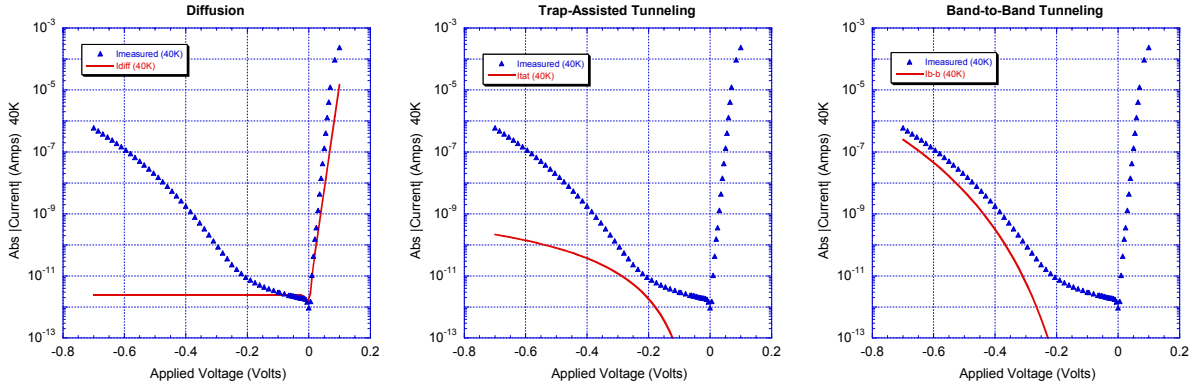

A **B** **C**

Fig. 5. Measured and modeled I-V data at 40K for the IR detector diode shown in figure 2. A. Measured data (solid triangles) and modeled diffusion current (solid line). B. Measured data as in A with modeled trap-assisted tunneling (TAT) current (solid line). C. Modeled band-to-band (BTB) tunneling (solid line).

The output from the modeling program at 40K for this particular diode is shown in Table 1. The output parameters include the "fit variance", which is a measurement of the chi-squared error between the data and the fitted function. As can be seen in the table, the avalanche breakdown terms were not included in this particular model fit, as they did not significantly reduce the corresponding chi-squared error. The generation-recombination terms are also absent from table 1, as they were found to be unnecessary to model the I-V curves measured on long wavelength detector diodes.

It is clear from figure 6 that at 78K the current is limited by diffusion at a reverse bias of 300mV, and at 40K, the same sample is limited by tunneling. This is mainly due to the drastic decrease in the intrinsic carrier concentration between the two temperatures, which minimizes the diffusion current at lower temperatures. It is expected that at low enough temperatures, the TAT influence would disappear due to freeze-out, and band-to-band tunneling would dominate.

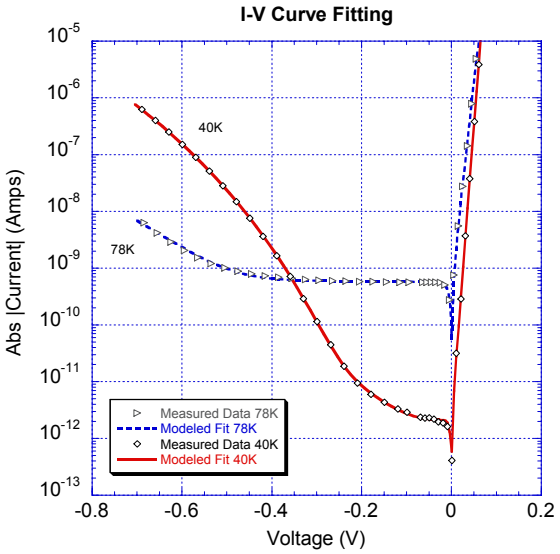

Fig. 6. I-V curve data and model fit for the detector diode shown in figures 2 and 5 at temperatures of 78K and 40K.

Parameter Name	Parameter Value	Uncertainty
Voltage Offset	-3.971E-03	8.751E+02
Saturation Current	2.136E-12	1.144E-12
Ideality Factor	1.231E+00	7.003E-02
Series Resistance	7.773E+01	2.181E+01
Shunt Resistance	1.203E+12	4.568E+12
Band-to-Band Tunneling Amplitude	3.472E+07	1.065E+07
Band-to-Band Tunneling Exponent	3.016E-01	9.650E-03
Band-to-Band Tunneling Rate	2.859E+01	2.623E-01
Band-to-Band Tunneling Onset V	-2.390E-01	1.500E-02
Avalanche Breakdown Voltage	-	-
Avalanche Breakdown Exponent	-	-
Avalanche Breakdown Onset V	-	-
Trap-Assisted Tunneling Amplitude	9.857E-09	1.176E-08
Trap-Assisted Tunneling Rate	3.823E+00	5.532E-01
Built-In Voltage	6.000E-02	-
Fit Variance	3.306E-02	-
R0	1.966E+09	1.084E+09
Tunneling/Ideal Ratio at -100 mV	3.261E-01	-
Tunneling/Ideal Ratio at -200 mV	3.051E+00	-
Minimum Reverse Voltage	-7.040E-01	-
Maximum Forward Voltage	9.603E-02	-
Test Date		-
Hybrid ID		-

Table 1. I-V Model program output for diode shown in figures 2, 5, and 6 at 40K.

At RVS, each HgCdTe wafer processed has test structure mini-arrays patterned on it which undergo routine I-V characterization as one method to evaluate the wafer performance. This data is stored in a sophisticated database which can be sorted by any number of operator criteria. This model has been applied to each set of I-V curves in this database, yielding a significant statistical representation of the various current limiting mechanisms operating on the devices produced at RVS. Once this modeling program has been applied to a detector diode, the modeled parameters may be used to extract information regarding the traps.

Using equations 12 and 13, the trap energy E_t' and density N_t has been calculated for 3780 long-wave IR $Hg_{1-x}Cd_xTe$ detector diodes from a variety of wafers at a temperature of 40K. The probability distribution of these calculated trap energies and densities are shown in figure 7. The range of calculated trap energy positions (filled triangles figure 7 left plot) span almost the entire bandgap, which was rather unexpected. It may be that the uncertainty in the parameters necessary for this calculation renders these values useless. Other authors have bypassed this problem by assuming a fixed trap level energy of seventy percent of the Fermi level. At 40K, the Fermi level in long wavelength detector diodes often lies just above the conduction band minimum, hence $E_t' = 0.7*E_F \sim 0.7*E_g$. This has also been calculated for these parts, and is included in the left plot of figure 7 as the open squares. This change has little impact on the calculated trap density shown in the right plot of figure 7. The median (50^{th} percentile) trap density shows an approximate $N_t=10^{10}cm^{-3}$ well below the intentional doping level the n-type base layer for these parts. The highest 5% which exhibit trap densities above this intentional doping level most likely suffer from very large leakage currents due to trap-assisted-tunneling, and may also suffer from compensation depending upon the charge state and lattice position of the trap. Shunted diodes may also give artificially enhanced trap-assisted tunneling amplitudes corresponding to an unreasonably high trap density.

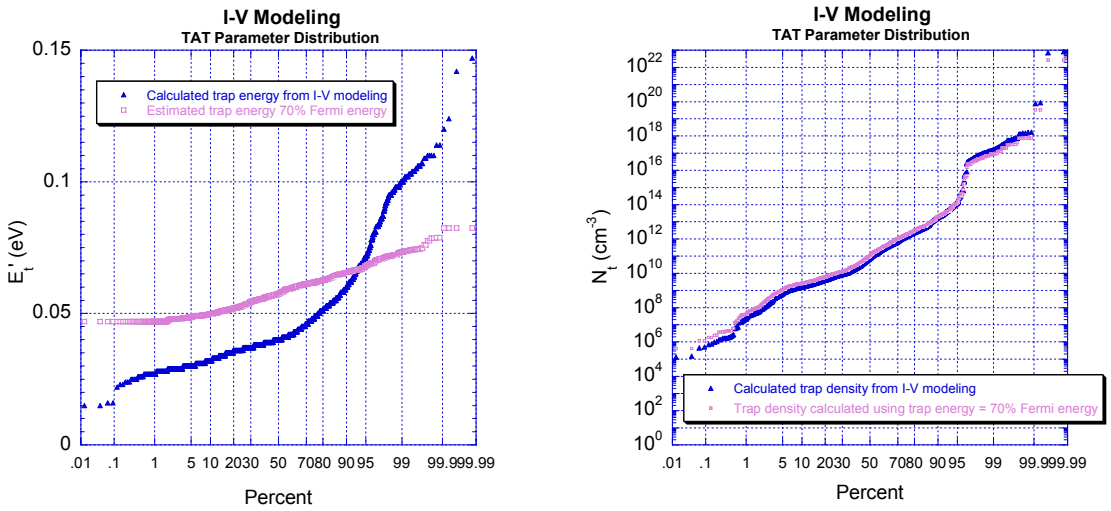

Fig. 7. Probability distributions of trap energy level E_t' (left) and trap density N_t (right) extracted from the modeled trap-assisted tunneling parameters for 3780 LWIR detectors at 40K. Open squares are estimates using $E_t' = 0.7*E_F$.

5. SUMMARY AND CONCLUSIONS

A sophisticated I-V modeling program has been developed that can reveal the dominant current limiting mechanisms in HgCdTe infrared detectors at various temperatures. This program has been applied to VLWIR detectors confirming that tunneling is a major concern for these devices. Furthermore, it was shown that quantification of the trap-assisted-tunneling trap sites is possible through careful analysis of the data. If the trapping density becomes comparable to the doping density, the diode electrical properties will become dependent upon the undesired trap properties. As doping concentrations are lowered in an attempt to reduce noise, the density of trapping sites becomes a major concern in these devices. This technique provides a quick method to estimate the trapping density in a detector diode. The broad applicability and ease of implementation combined with the usefulness of this program suggest that it will become an important tool in IR detector analysis.

ACKNOWLEDGEMENTS

The authors of this paper would like to gratefully acknowledge Murray Welkowsky and David Acton for their support and discussions.

REFERENCES

1. P.R. Bevington and D. K. Robinson, *Data Reduction and Error Analysis for the Physical Sciences*, 2nd Ed., WCB/McGraw-Hill, 1992.
2. S.M. Sze, *Physics of Semiconductor Devices*, 2nd Ed., John Wiley & Sons, 1981.
3. A. G. Chynoweth, W. L. Feldmann, C. A. Lee, R. A. Logan, and G. L. Pearson, *Phys. Rev.* **118,** p. 425, 1960.
4. G. L. Hansen and J. L. Schmit, *J. Appl. Phys*. **54**(3), p. 1639, 1983.
5. A. G. Chynoweth, W. L. Feldmann and R. A. Logan, *Phys. Rev.* **121**, p. 684, 1961.
6. P. J. Price *Bull. Am. Phys. Soc*. **5**, p. 406, 1960.

7. Sah, C. T. *Phys. Rev.* **123**, p. 1594-1612, 1961.
8. M. A. Kinch, edited by R. K. Williardson and A. C. Beer, *Semiconductors and Semimetals Volume 18*, Chap. 7, Academic, New York, 1981.
9. Y. Nemirovsky, D. Rosenfeld, R. Adar, and A. Kornfeld, "Tunneling and dark currents in HgCdTe photodiodes", *J. Vac. Sci. Technol.* **A7**(2), p. 528, 1989.
10. Y. Nemirovsky, R. Fastow, M. Meyassed and A. Unikovsky, *J. Vac. Sci. Technol.* **B9** (1991) 1829-39.
11. Y. Nemirovsky and A. Unikovsky, *J. Vac. Sci. Technol.* **B10**, p. 1602-1610, 1992.
12. S. K. Singh, V. Gopal, R. K. Bhan and V. Kumar, "An analysis of the dynamic resistance variation as a function of reverse bias voltage in a HgCdTe diode", *Semicond. Sci. Technol*. **15**, p. 752-755, 2000.
13. D. Rosenfeld and G. Bahir, *IEEE Transactions on Electron Devices*. **39**(7), p. 1638-1645, 1992.
14. V. Gopal, S. K. Singh and R. M. Mehra, *Semicond. Sci. Technol.* **16**, p. 372-376, 2001.